


# Simulation of vibrational dynamics using qubits and qudits

Erik Lötstedt <sup>1,2,3,\*</sup> and Kaoru Yamanouchi <sup>2,4</sup>

<sup>1</sup>*RIKEN iTHEMS, 2-1 Hirosawa, Wako, Saitama 351-0198, Japan*

<sup>2</sup>*Trapped Ion Quantum Computer Team, TRIP Headquarters,  
RIKEN, 2-1 Hirosawa, Wako, Saitama 351-0198, Japan*

<sup>3</sup>*Computational Condensed Matter Physics Laboratory,  
RIKEN Pioneering Research Institute (PRI),*

*2-1 Hirosawa, Wako, Saitama 351-0198, Japan*

<sup>4</sup>*Institute for Attosecond Laser Facility,  
The University of Tokyo, 7-3-1 Hongo,  
Bunkyo-ku, Tokyo 113-0033, Japan*

(Dated: May 14, 2026)

## Abstract

We investigate the quantum computing of the vibrational dynamics of CO<sub>2</sub> and H<sub>2</sub>O by constructing the vibrational Hamiltonian in qubit and qudit form by two types of qubit encodings (binary and direct) and a qudit encoding. We simulate the time-dependent vibrational population transfer using the three different encodings, including the effect of noise and find that the qudit encoding leads to the most accurate results both for CO<sub>2</sub> and H<sub>2</sub>O because of the small number of terms in the qudit Hamiltonian as long as the same values of the entangling gate error rates are adopted.

---

\* loetstedte@riken.jp

## I. INTRODUCTION

A quantum computer is usually constructed from qubits, quantum two-level systems having a ground state,  $|0\rangle$ , and an excited state,  $|1\rangle$ . Currently, there are several types of qubit-based quantum computers in operation, including devices where the qubits are realized as superconducting circuits [1], trapped ions [2, 3], and neutral atoms [4–6]. The number of qubits  $N_q$  is at present around  $N_q = 150$  for superconducting-type quantum computers [7],  $N_q = 100$  for trapped-ion type quantum computers [8], and about  $N_q = 300$  for neutral-atom type quantum computers [5].

Qubit-based quantum computers have been employed for pioneering applications in quantum chemistry [9–12], where the electronic energies of small molecules such as  $\text{H}_2\text{O}$  [13] and  $\text{F}_2$  [14] were calculated. However, because of the noise present on current quantum computers, and because of the large number of terms in the qubit form of the electronic Hamiltonian [15], quantum computing of large molecules is still difficult. A possible way forward is the quantum-centric supercomputing approach [16], in which quantum computers are combined with supercomputers. A representative method is the quantum-selected configuration interaction method, in which the active configuration space is determined by sampling from a wave function prepared by a quantum computer and the electronic energy is obtained by the solution of the corresponding eigenvalue problem on a classical supercomputer [17–19].

Another promising approach is the use of qudits as a basic unit of quantum computing [20–22]. A qudit is a  $d$ -level quantum system with states

$$|\ell\rangle = |0\rangle, |1\rangle, \dots, |d-1\rangle. \quad (1)$$

A quantum computer constructed from  $N_q$  qudits is in a superposition of  $d^{N_q}$  states, which is exponentially larger than the  $2^{N_q}$  states available in a qubit-based quantum computer. Qudit-based quantum computers having up to around ten qudits have been realized with superconducting circuits [23–28], trapped ions [29–38], photonic circuits [39–41], donor atoms [42], neutral atoms [43–45], and vacancy centers [46, 47]. Trapped-ion setups are particularly promising because of the long coherence time and the high-fidelity gate operations. So far, different values of  $d$  were adopted depending on the atomic ion species:  $d = 8$  in  $^{40}\text{Ca}^+$  [31],  $d = 13$  in  $^{137}\text{Ba}^+$  [37], and  $d = 4$  in  $^{171}\text{Yb}^+$  [32, 38].

Several advantages of using qudits for quantum computation have been proposed, including the simulation of fermions [48], chemical dynamics [49], lattice gauge theory [36], and spin dynamics [30, 34], simplifications of multi-qubits gates [40, 50] and the reduction of the circuit depth [50–52]. Qudits may also be used in error correction [53–55]. Indeed, a logical qudit ( $d = 3$  and  $4$ ) encoded using the Gottesman-Kitaev-Preskill bosonic code [56] was demonstrated to have an effective lifetime longer than a physical qudit by a factor of about two [57].

In the present study, we show that qudits are advantageous for the simulation of molecular vibration. Because a nonlinear  $N$ -atomic molecule has  $3N - 6$  vibrational modes, the calculation of the vibrational energy levels of a molecule is a hard computational problem. If we assume that each vibrational mode is described by  $K$  basis functions, the number of expansion coefficients in the vibrational wave function becomes  $K^{3N-6}$ , which increases exponentially with increasing  $N$ . Although quantum computing of molecular vibration has attracted less attention compared to the quantum computing of the electronic structure of molecules, theoretical rovibrational spectroscopy is recognized as one of the areas in which quantum computers are expected to be useful [10]. Several attempts have been made to evaluate vibrational energies using qubit-based quantum computers [58–67], but demonstrations using quantum hardware have so far been limited to few-atomic molecules such as  $\text{CO}_2$  [61, 62, 65, 68],  $\text{H}_2\text{O}$  [66], and  $\text{NH}_3$  [65].

We demonstrate that the qudit representation of the vibrational Hamiltonian has much fewer terms than the qubit representation, and consequently, a qudit quantum circuit for the Suzuki-Trotter approximation of the time evolution operator contains much fewer two-qudit gates than the number of two-qubit gates in the corresponding qubit quantum circuit, resulting in much smaller error originating from the noise. We then assess quantitatively the qudit advantage over qubits for simulation of vibrational dynamics on noisy quantum computers by carrying out quantum computing of  $\text{CO}_2$  and  $\text{H}_2\text{O}$  using a completely depolarizing noise model.

## II. THEORY

### A. Vibrational Hamiltonian

We consider the vibrational Hamiltonian of a general nonlinear molecule,

$$H = H_{\text{HO}} + H_{\text{AH}}, \quad (2)$$

where

$$H_{\text{HO}} = \sum_{k=1}^{N_m} H_{\text{HO}}^{(k)} = \sum_{k=1}^{N_m} \frac{\omega_k}{2} \left( -\frac{\partial^2}{\partial q_k^2} + q_k^2 - 1 \right) \quad (3)$$

is the harmonic oscillator part defined in terms of the dimensionless normal mode coordinates  $q_k$ ,  $N_m$  is the number of modes, and

$$H_{\text{AH}} = \sum_{\substack{j,k,l=1 \\ j \leq k \leq l}}^{N_m} f_{jkl} q_j q_k q_l \quad (4)$$

defines the anharmonic potential in terms of the anharmonic coupling constants  $f_{jkl}$  ( $j, k, l = 1, 2, \dots, N_m$ ). In the current investigation, we consider anharmonic coupling up to third order in  $q_k$ , but in the general case, the anharmonic potential (4) may contain terms of the fourth and higher orders [69].

The time-dependent vibrational wave function is expanded according to

$$|\psi(t)\rangle = \sum_{v_1, v_2, \dots, v_{N_m}=0}^{v_{\text{max}}} c_{\mathbf{v}}(t) |\mathbf{v}\rangle, \quad (5)$$

where  $v_k$  is the vibrational quantum number of the  $k$ th mode,  $\mathbf{v} = (v_1, v_2, \dots, v_{N_m})$  is a composite index,  $v_{\text{max}}$  is the maximum vibrational quantum number, and

$$|\mathbf{v}\rangle = |v_1\rangle |v_2\rangle \cdots |v_{N_m}\rangle \quad (6)$$

is a direct product of  $N_m$  harmonic-oscillator eigenstates  $|v_k\rangle$ . The basis functions  $|\mathbf{v}\rangle$  are eigenfunctions of  $H_{\text{HO}}$ ,

$$H_{\text{HO}} |\mathbf{v}\rangle = \left( \sum_{k=1}^{N_m} v_k \omega_k \right) |\mathbf{v}\rangle, \quad (7)$$

but not of the total Hamiltonian  $H$  because of the anharmonic coupling  $H_{\text{AH}}$ .

## B. Qubit and qudit encodings

In order to encode the basis states as qubit states, we consider two different encoding schemes, i.e., the binary encoding [70] and the direct encoding [70]. In the binary encoding, we map a basis state to a qubit state according to

$$|\mathbf{v}\rangle = |\text{bin}(v_1) \text{bin}(v_2) \cdots \text{bin}(v_{N_m})\rangle_{\text{q}}, \quad (8)$$

where  $\text{bin}(v)$  is the binary representation of the integer  $v$ . The binary encoding requires  $N_{\text{q}} = N_m \lceil \log_2(v_{\text{max}} + 1) \rceil$  qubits, where  $\lceil \cdot \rceil$  is the ceiling function. For example, a two-mode basis state  $|v_1 = 0, v_2 = 3\rangle$  is represented as the qubit state  $|\text{bin}(0) \text{bin}(3)\rangle_{\text{q}} = |0011\rangle_{\text{q}}$ . In the case when  $v_{\text{max}} + 1$  is not equal to a power of 2, some qubit states do not represent vibrational basis states and are not used in the encoding.

In the direct encoding (also referred to as the unary encoding [70] or one-hot encoding [71]), we map a single-mode basis state  $|v\rangle$  to a qubit state where the  $v$ th qubit is in the excited state, and the rest of the qubits are in the ground state,

$$|v\rangle = X_v |\bar{0}\rangle_{\text{q}}, \quad (9)$$

where  $X_v$  is a Pauli  $\sigma_x$  operator acting on the  $v$ th qubit, and  $|\bar{0}\rangle_{\text{q}} = |0 \cdots 00\rangle_{\text{q}}$  is the all-zero qubit state. The multi-mode basis state  $|\mathbf{v}\rangle$  is encoded accordingly as

$$|\mathbf{v}\rangle = \prod_{k=1}^{N_m} X_{\mu(k)} |\bar{0}\rangle_{\text{q}}, \quad \mu(k) = (k-1)(v_{\text{max}} + 1) + v_k. \quad (10)$$

The direct encoding requires  $N_{\text{q}} = N_m(v_{\text{max}} + 1)$  qubits. Only a small fraction  $[(v_{\text{max}} + 1)/2^{v_{\text{max}}+1}]^{N_m}$  of the total number of qubit states is employed.

In the case of qudits, we map each harmonic oscillator basis function  $|v\rangle$  to a qudit state  $|\ell\rangle_{\text{q}}$ ,

$$|\mathbf{v}\rangle = |\ell_1 \ell_2 \cdots \ell_{N_m}\rangle_{\text{q}}, \quad \ell_k = v_k, \quad (11)$$

which requires  $N_m$  qudits having  $d = v_{\text{max}} + 1$  levels.

The qubit or qudit Hamiltonian is expressed as

$$H_{\text{q}} = \sum_{n=1}^{L_{\text{q}}} h_n \Gamma_n, \quad (12)$$

where  $h_n$  is a numerical coefficient, and  $\Gamma_n$  is defined as a direct product of generalized Gell-Mann matrices  $\lambda_j$  [72],

$$\Gamma_n = \lambda_{j_{n(N_q-1)}} \lambda_{j_{n(N_q-2)}} \cdots \lambda_{j_{k0}}, \quad (13)$$

where  $j_{nm} \in \{0, \dots, d^2-1\}$  indicates the index of the Gell-Mann matrix operating on the  $m$ th qudit. The generalized Gell-Mann matrices  $\lambda_j$  are a convenient basis for qudit operators [31]. They are of size  $d \times d$ , and have the properties  $\text{tr}(\lambda_j) = 0$  and  $\text{tr}(\lambda_j \lambda_k) = 2\delta_{jk}$ . When  $d = 2$ ,  $\lambda_j$  become the standard Pauli matrices:  $\lambda_0(d = 2) = I$ ,  $\lambda_1(d = 2) = X$ ,  $\lambda_2(d = 2) = Y$ , and  $\lambda_3(d = 2) = Z$ . The detailed definition of  $\lambda_j$  employed in this paper can be found in Appendix B of Ref. [73]. Note however that in this paper, we label the generalized Gell-Mann matrices starting from  $j = 0$  instead of from  $j = 1$  in [73].

The numerical coefficients  $h_n$  are obtained in two steps. First, we derive the qubit (or qudit) representation of the single-mode operators  $H_{\text{HO}}^{(k)}$  [see Eq. (3)] and  $q^\kappa$  ( $\kappa = 1, 2, 3$ ) according to

$$o^{(1)} = \sum_{n=1}^{L_q^{(1)}} h_n^{(1)} \Gamma_n^{(1)}, \quad h_n^{(1)} = 2^{-\frac{N_q}{N_m}} \text{tr}(o^{(1)} \Gamma_n^{(1)}), \quad (14)$$

where  $o^{(1)}$  is  $H_{\text{HO}}^{(k)}$  or  $q^\kappa$ , and  $\Gamma_n^{(1)}$  acts on  $\frac{N_q}{N_m}$  qubits (or on one qudit). Second, the expansion of the complete  $N_m$ -mode operator is obtained as a product of the expansions in (14). For example, the qubit representation of the operator  $q_1 q_2 q_3$  is

$$(q_1 q_2 q_3)_q = \sum_{n_1, n_2, n_3=1}^{L_q^{(1)}} h_{n_1}^{(1)} h_{n_2}^{(1)} h_{n_3}^{(1)} \Gamma_{n_1}^{(1)} \Gamma_{n_2}^{(1)} \Gamma_{n_3}^{(1)}, \quad (15)$$

where  $h_n^{(1)}$  and  $\Gamma_n^{(1)}$  are derived in (14) with  $o^{(1)} = q$ . Third, the qubit representations of  $H_{\text{HO}}$  and  $q_j q_k q_l$  are combined to generate the expansion (12) for the complete Hamiltonian  $H_q$ .

In order to compare the qubit Hamiltonians in the different encodings with the qudit Hamiltonian, we define the operator order  $\Omega(\Gamma_n)$  as the number of qubits or qudits that  $\Gamma_n$  acts non-trivially on. We use  $L_q(\Omega)$  to denote the number of terms in (12) having an operator order  $\Omega$ .

### C. Time evolution by the Suzuki-Trotter approximation

Given the qubit or qudit representation (12), we calculate a time-dependent density matrix  $\rho(t)$  by the Suzuki-Trotter approximation [74, 75],

$$\rho(t) = U^{N_{\text{ST}}} \rho_0 U^{\dagger N_{\text{ST}}}, \quad (16)$$

where  $N_{\text{ST}}$  is the number of Suzuki-Trotter steps,  $\rho_0$  is the initial state, and

$$U = \prod_{n=1}^{L_q} e^{-i\Delta t h_n \Gamma_n / \hbar} \quad (17)$$

is the first-order Suzuki-Trotter time evolution operator. We use a pure, uncorrelated initial state,

$$\rho_0 = |\mathbf{v}_0\rangle\langle\mathbf{v}_0|, \quad (18)$$

and aim to compute the time-dependent populations  $p_{\mathbf{v}}(t)$ , defined as the diagonal elements of  $\rho(t)$ ,

$$p_{\mathbf{v}}(t) = \langle\mathbf{v}|\rho(t)|\mathbf{v}\rangle. \quad (19)$$

The exact populations obtained without the Suzuki-Trotter approximations at a certain value of  $v_{\text{max}}$  can be expressed as

$$\begin{aligned} p_{\mathbf{v}}^{\text{exact}}(t) &= |\langle\mathbf{v}|e^{-itH/\hbar}|\mathbf{v}_0\rangle|^2 \\ &= \sum_{m,n} e^{-it(E_m - E_n)/\hbar} \alpha_{mn}^{\mathbf{v}\mathbf{v}_0}, \end{aligned} \quad (20)$$

where the coefficient  $\alpha_{mn}^{\mathbf{v}\mathbf{v}_0}$  is defined as

$$\alpha_{mn}^{\mathbf{v}\mathbf{v}_0} = \langle\psi_m|\mathbf{v}_0\rangle\langle\mathbf{v}_0|\psi_n\rangle\langle\psi_n|\mathbf{v}\rangle\langle\mathbf{v}|\psi_m\rangle, \quad (21)$$

$|\psi_n\rangle$  is an approximate eigenfunction of  $H$  defined as

$$|\psi_n\rangle = \sum_{\mathbf{v}} \psi_{\mathbf{v}n} |\mathbf{v}\rangle, \quad (22)$$

and  $\psi_{\mathbf{v}n}$  is an eigenfunction of the matrix representation of  $H$  satisfying

$$E_n \psi_{\mathbf{v}n} = \sum_{\mathbf{v}', \dots, \mathbf{v}'_{N_m}=0}^{v_{\text{max}}} \langle\mathbf{v}|H|\mathbf{v}'\rangle \psi_{\mathbf{v}'n}. \quad (23)$$

In order to simulate the noise due to the decoherence, present in all currently available quantum computers, we employ the completely depolarizing channel [76]. After each application of the unitary operation  $e^{-i\Delta t h_n \Gamma_n / \hbar}$ , we evolve  $\rho(t)$  according to

$$\rho(t) \rightarrow \epsilon_n \frac{\mathbb{I}}{d^{N_q}} + (1 - \epsilon_n) \rho(t), \quad (24)$$

where  $\mathbb{I}$  is the  $d^{N_q} \times d^{N_q}$  identity matrix ( $d = 2$  for qubits and  $d > 2$  for qudits), and  $\epsilon_n$  is the gate error. We use a simple error model where the gate error  $\epsilon_n$  is defined as

$$\epsilon_n = \begin{cases} 0 & \text{if } \Omega(\Gamma_n) = 1, \\ [2\Omega(\Gamma_n) - 3]\epsilon_{2q} & \text{if } \Omega(\Gamma_n) > 1, \end{cases} \quad (25)$$

where  $\epsilon_{2q}$  is the two-qubit gate error. The gate error  $\epsilon_n$  is set to zero when the operator order  $\Omega(\Gamma_n) = 1$  because the single-qubit gate error is typically more than one order of magnitude smaller than the two-qubit gate error. For example, on Quantinuum's recent 98-qubit Helios trapped-ion device [8], the single-qubit error is  $\epsilon_{1q} \approx 3 \times 10^{-5}$ , and  $\epsilon_{2q} \approx 8 \times 10^{-4}$ . The error for a multi-qubit or qudit gate is set to  $[2\Omega(\Gamma_n) - 3]\epsilon_{2q}$  because an  $\Omega$ -qubit ( $\Omega \geq 2$ ) Pauli rotation gate can be decomposed into  $2\Omega - 3$  two-qubit gates [77]. On existing quantum computers, only one- and two-qubit gates are implemented. The model (25) accounts for the decomposition of a multi-qubit gate into single- and two-qubit gates before executing the quantum circuit.

Even in the absence of noise ( $\epsilon_{2q} = 0$ ), the Suzuki-Trotter approximation defined in Eqs. (16) and (17) implies an algorithmic error

$$|e^{-i\Delta t H_q / \hbar} - U| \approx \varepsilon_{\text{ST}} = \frac{\Delta t^2}{2\hbar^2} \left| \sum_n^{L_q} \sum_{m=n+1}^{L_q} h_n h_m [\Gamma_n, \Gamma_m] \right|, \quad (26)$$

where  $[\cdot, \cdot]$  is the commutator and we assume that  $\Delta t$  is small. Because the signs of the different terms in the sum on the right hand side in Eq. (26) can be changed by changing the order of the terms in the expansion (12), the Suzuki-Trotter error depends on the order of the terms in (12). We have applied the following simplified method for optimizing the order of the terms in the Suzuki-Trotter expansion. First, we compute the commutator score

$$s_n = \sum_{m=1}^{L_q} |h_n h_m [\Gamma_n, \Gamma_m]|, \quad (27)$$

where  $|\cdot|$  refers to the Frobenius norm. We then define an initial ordering by sorting the terms  $h_n \Gamma_n$  in order of decreasing  $s_n$ . In order to minimize the error  $\varepsilon_{\text{ST}}$ , we sequentially

check the terms  $h_n\Gamma_n$  from  $n = 1$  to  $n = L_q - 1$  and change the order if a local swap  $h_n\Gamma_n \leftrightarrow h_{n+1}\Gamma_{n+1}$  lowers the value of  $\varepsilon_{\text{ST}}$ . We repeat the local swapping until  $\varepsilon_{\text{ST}}$  is not further lowered, and use this final ordering in the Suzuki-Trotter simulations. Although this simple optimization method does not guarantee the best ordering, it results in a small Suzuki-Trotter error where the populations obtained using the Suzuki-Trotter approximation differ from the exact populations by less than 0.1 (see Sec. III), and ensures that the first-order Suzuki-Trotter approximation (17) is of similar accuracy for all three encoding schemes (binary, direct, and qudit). An extended discussion of the operator ordering in the Suzuki-Trotter approximation can be found in [78–80].

### III. RESULTS

#### A. Two-mode model of CO<sub>2</sub>

In this section, we compare the three different encoding schemes, qubit binary, qubit direct, and qudit by carrying out time-dependent Suzuki-Trotter simulations of population dynamics in a two-mode ( $N_m = 2$ ) model of CO<sub>2</sub> with the symmetric stretch ( $\nu_1$ ) and bending ( $\nu_2$ ) modes. This model is the same as that we employed in our previous investigations [61, 62]. The numerical values of the harmonic frequencies  $\omega_k$  and the anharmonic constants  $f_{jkl}$  taken from [81] are  $\omega_1 = 1354.31 \text{ cm}^{-1}$ ,  $\omega_2 = 672.85 \text{ cm}^{-1}$ ,  $f_{111} = -45.78 \text{ cm}^{-1}$ , and  $f_{122} = 74.72 \text{ cm}^{-1}$  (all other  $f_{jkl} = 0$ ).

CO<sub>2</sub> features a well-known anharmonic resonance, referred to as a Fermi resonance [82, 83], where the singly excited symmetric stretching mode is strongly coupled to the doubly excited bending mode. The strong coupling arises from the non-zero value of the anharmonic coupling  $f_{122}$  ( $= 74.72 \text{ cm}^{-1}$  in our model) and because  $2\omega_2 \approx \omega_1$ . The Fermi doublet refers to the pair of states having approximate wave functions  $|\psi_{\text{Fermi}\pm}\rangle \approx (|10\rangle \pm |02\rangle)/\sqrt{2}$ , separated in energy by approximately  $f_{122}$ .

##### 1. Qubit and qudit Hamiltonians

In Fig. 1(a), we show the number of terms  $L_q$  in the expansion (12) of the qubit and qudit Hamiltonians for CO<sub>2</sub>. We can see Fig. 1 that  $L_q$  increases approximately as a quadratic function of  $v_{\text{max}}$  for the qubit direct and qudit encodings. We find that in the range  $v_{\text{max}} \leq 7$

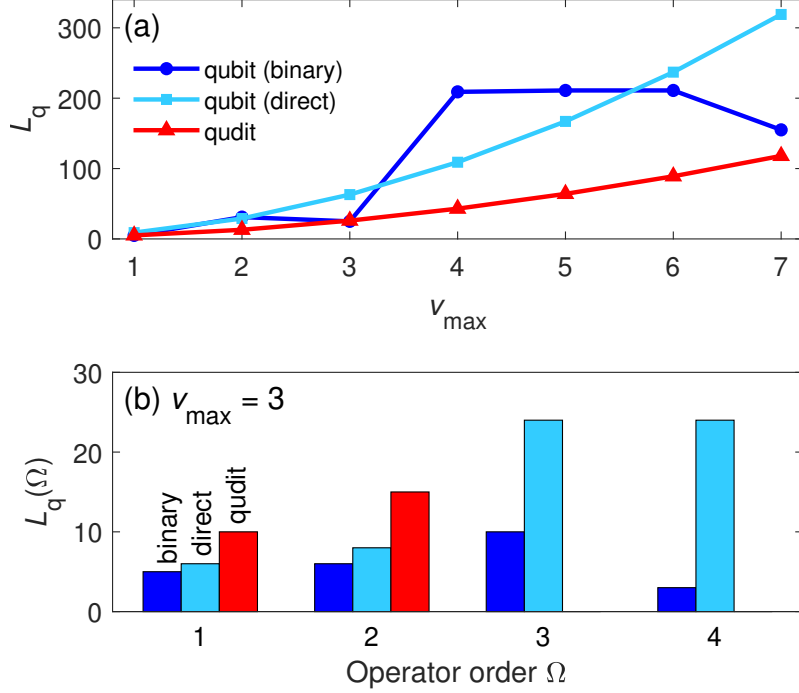


FIG. 1. (a) Number of terms  $L_q$  in the qubit/qudit Hamiltonian for the two-mode CO<sub>2</sub> model. The binary, direct, and qudit encodings are compared. (b) Breakdown of  $L_q$  into the number of terms of different operator order  $\Omega$ , for a maximum vibrational quantum number  $v_{\max} = 3$ .  $\Omega$  is defined as the number of qubits or qudits an operator acts non-trivially on. We have  $L_q(3) = L_q(4) = 0$  for the qudit encoding because the number of qudits is  $N_q = 2$ .

shown in Fig. 1,  $L_q$  for the direct and qudit encodings can be fitted approximately to  $L_q \approx av_{\max}^2$  with  $a \approx 6.59$  for the direct encoding and  $a \approx 2.47$  for the qudit encoding. The reason for the approximately quadratic increase of  $L_q$  with increasing  $v_{\max}$  is that we have two modes, and the number of non-zero matrix elements of single mode operators like  $q$ ,  $q^2$ , and  $q^3$  increases linearly with increasing  $v_{\max}$ . On the other hand, the number of terms  $L_q$  in the binary encoding displays a non-monotonic  $v_{\max}$ -dependence.  $L_q$  takes a small value when  $v_{\max} + 1$  can be expressed as a power of 2, that is, at  $v_{\max} = 3$  and 7, something which is an intrinsic feature of the binary encoding [70]. When  $v_{\max} + 1 = 2^\eta$  with an integer  $\eta$ , all qubit states represent vibrational basis states.

In Fig. 1(b), we show the number of terms in the qubit/qudit Hamiltonians at each operator order  $\Omega$ , for  $v_{\max} = 3$ . While the qudit Hamiltonian contains only single- and two-qudit operators ( $\Omega = 1$  and 2), both the binary and direct qubit Hamiltonians contain terms

with operator orders three and four. Because more than one qubit is used to represent one vibrational mode in the binary and direct encodings, many-qubit operators are required to represent both the anharmonicity of a single mode (terms like  $q_1^3$  in  $H_{\text{AH}}$ ) as well as the anharmonic coupling between the two modes. In the case of the qudit encoding, where one mode is encoded in one qudit, the intra-mode anharmonic coupling is implemented by single-qudit operators, and the inter-mode couplings are implemented by two-qudit operators.

Because the major source of noise in currently available quantum computers is the two-qubit gates, a smaller number of two-qubit or two-qudit gates results in more accurate (less noise-prone) simulations. Assuming that a Pauli rotation gate  $\exp(-i\Delta t h_n \Gamma_n / \hbar)$  can be decomposed into  $2\Omega(\Gamma_n) - 3$  two-qubit gates as discussed below Eq. (25), we obtain at  $v_{\text{max}} = 3$  the number of two-qubit gates in the binary encoding, the number of two-qubit gates in the direct encoding, and the number of two-qudit gates in one Suzuki-Trotter step as

$$\begin{aligned}\Lambda_{2q}(\text{binary}) &= 51, \\ \Lambda_{2q}(\text{direct}) &= 200, \text{ and} \\ \Lambda_{2q}(\text{qudit}) &= 15.\end{aligned}\tag{28}$$

Note that we do not account for circuit transpilation, which may change the two-qubit gate count depending on the qubit layout on a particular quantum device [84, 85]. As is clear from Eq. (28), the qudit encoding results in much fewer two-qudit gates than the binary and direct encodings, and we therefore expect that the qudit encoding leads to more accurate population dynamics.

## 2. Time-dependent vibrational dynamics

In Fig. 2, we show an example of the time-dependent population  $p_{v_1 v_2=10}(t)$  in the two-mode  $\text{CO}_2$  model at  $v_{\text{max}} = 3$ , for which the number of terms in the binary qubit Hamiltonian,  $L_q(\text{binary}) = 25$ , and the qudit Hamiltonian,  $L_q(\text{qudit}) = 26$ , are almost equal. The total number of qubits required for  $v_{\text{max}} = 3$  is  $N_q(\text{binary}) = 4$  and  $N_q(\text{direct}) = 8$ . For the qudit simulation, we require two qudits having  $d = 4$ . The numerical values of  $h_n$  and the ordering of the terms in the Suzuki-Trotter approximation (17) are available at [86]. We employ the same value for the two-qubit gate error and the two-qudit gate error,  $\epsilon_{2q} = 10^{-3}$ . This value is similar to what is achieved in currently available qubit-based

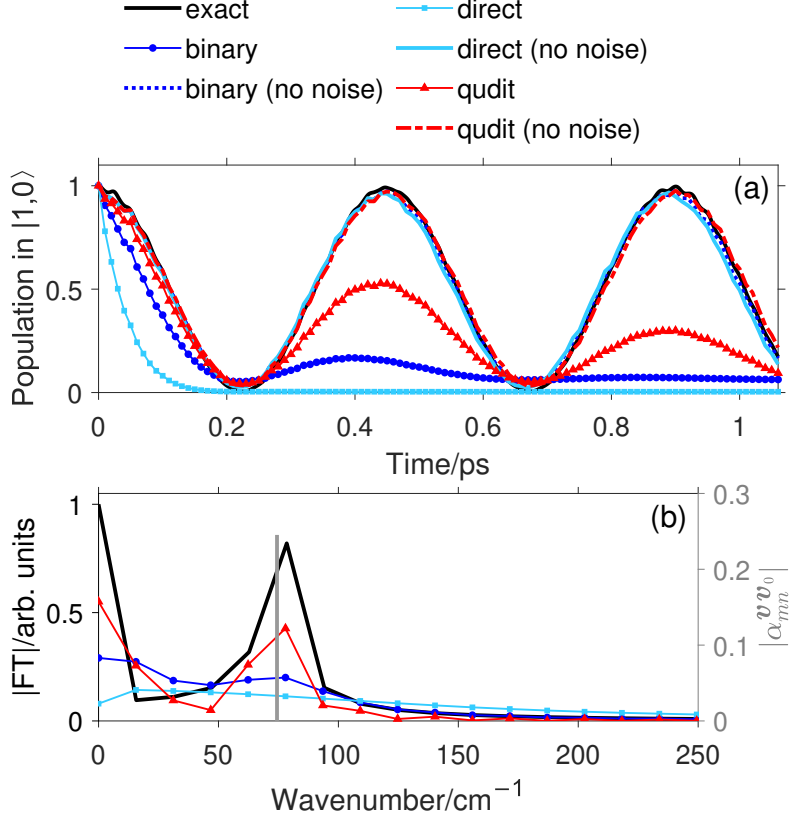


FIG. 2. (a) Time-dependent population  $p_{10}(t)$  in the  $|\mathbf{v}\rangle = |1,0\rangle$  state in the two-mode  $\text{CO}_2$  model with  $v_{\max} = 3$ . The initial state is  $|\mathbf{v}_0\rangle = |1,0\rangle$  and the Suzuki-Trotter step size is  $\Delta t = 0.01$  ps. (b) Normalized absolute value of the Fourier transform of the time-dependent populations in (a). The Fourier transform of the noiseless Suzuki-Trotter simulations are not shown because they are almost the same as as the exact curve. The vertical gray stick indicates the Fermi resonance energy difference  $\Delta E_{\text{Fermi}} = 74.4 \text{ cm}^{-1}$  obtained by matrix diagonalization of  $H_{\text{q}}$ . The length of the gray stick (numerical value indicated on the right-hand vertical axis) is given by the absolute value of the expansion coefficient  $\alpha_{mn}^{v v_0}$  [see Eq. (21)] in the exact population.

trapped-ion quantum computers [2, 8]. For qudit-based trapped-ion quantum computers, two-qudit gate errors ranging from about  $\epsilon_{2\text{q}} = 5 \times 10^{-2}$  [31, 38] to  $\epsilon_{2\text{q}} \approx 1 \times 10^{-2}$  [33] have been demonstrated.

The initial state is taken to be  $|\mathbf{v}_0\rangle = |1,0\rangle$ , corresponding to one of the basis states involved in the Fermi resonance. Because of the coupling between the  $|1,0\rangle$  and  $|0,2\rangle$  states, the population in  $|1,0\rangle$  is transferred to  $|0,2\rangle$  on a time scale  $2\pi\hbar/\Delta E_{\text{Fermi}}$ , where  $\Delta E_{\text{Fermi}}$  is the Fermi doublet energy splitting.

We can see in Fig. 2(a) that the exact population  $p_{10}^{\text{exact}}(t)$  (black solid curve) obtained without using the Suzuki-Trotter approximation and the populations obtained using the Suzuki-Trotter approximation with zero noise (dotted, solid, and dash-dotted curves) almost overlap, showing that the algorithmic error in the Suzuki-Trotter approximation is sufficiently small. We have  $|p_{10}^{\text{no noise}}(t) - p_{10}^{\text{exact}}(t)| < 0.08$  during the time range  $0 \leq t \leq 1$  ps for both the qubit and qudit encodings. The populations simulated using the completely depolarizing noise model decay because of the noise. According to the noise model (24), the noisy populations are approximately given by

$$\begin{aligned} p_{\mathbf{v}}^{\text{noisy}}(t) &\approx (1 - \epsilon_{2\text{q}})^{N_{\text{ST}}\Lambda_{2\text{q}}} p_{\mathbf{v}}^{\text{no noise}}(t) \\ &\approx e^{-\frac{t}{\tau}} p_{\mathbf{v}}^{\text{no noise}}(t), \end{aligned} \quad (29)$$

where the decay time  $\tau$  is given by

$$\tau = \frac{\Delta t}{\Lambda_{2\text{q}}\epsilon_{2\text{q}}}, \quad (30)$$

and  $\Lambda_{2\text{q}}$  is the number of two-qubit/qudit gates in one Suzuki-Trotter step. We obtain  $\tau_{\text{binary}} \approx 0.20$  ps,  $\tau_{\text{direct}} \approx 0.050$  ps, and  $\tau_{\text{qudit}} \approx 0.67$  ps for the time-dependent populations shown in Fig. 2.

In Fig. 2(b), we show the Fourier transform of the time-dependent population in Fig. 2(a). The exact and qudit Fourier spectra show a clear peak at  $74 \text{ cm}^{-1}$  (the Fermi resonance gap). The simulations performed using the qubit binary encoding results in a broad peak around  $74 \text{ cm}^{-1}$ , while no peak can be seen in the curve obtained using the qubit direct encoding, reflecting the fast decay time. The Fourier spectra in Fig. 2(b) suggest that we can retrieve energy differences by recording a time-dependent observable (a population, for example) and computing the Fourier transform, as is also clear from Eq. (20). This Fourier transform approach has been successfully implemented experimentally for the high-precision measurements of atomic and molecular transition energies [87, 88]. However, in order to derive vibrational energy differences with a resolution of  $\Delta\tilde{\nu} = 1 \text{ cm}^{-1}$  from the Fourier transform of a signal calculated on a quantum computer, we would need to continue the simulation until  $t \sim 2\pi/c\Delta\tilde{\nu} \approx 200$  ps, which is difficult at the currently realized error rate of  $\epsilon_{2\text{q}} \approx 10^{-3}$ .

While we have used the same value ( $\epsilon_{2\text{q}} = 10^{-3}$ ) of the two-qubit/qudit gate error for both qubit and qudit simulations in Fig. 2, resulting in a longer decay time  $\tau$  for qudits, we can use Eq. (30) to estimate the two-qudit gate error  $\epsilon_{2\text{q}}^{\text{qudit}}$  for which the decay time

becomes the same for qubit and qudit quantum computers. Assuming the same value of  $\Delta t$  for qubits and qudits, we should have

$$\epsilon_{2q}^{\text{qudit}} = \frac{\Lambda_{2q}^{\text{qubit}}}{\Lambda_{2q}^{\text{qudit}}} \epsilon_{2q}^{\text{qubit}} \quad (31)$$

for obtaining  $\tau_{\text{qudit}} = \tau_{\text{qubit}}$ . Using  $\Lambda_{2q}^{\text{qubit}} = \Lambda_{2q}(\text{binary})$  from Eq. (28), and assuming the currently realized value  $\epsilon_{2q}^{\text{qubit}} = 10^{-3}$  for the two-qubit gate error, we obtain  $\epsilon_{2q}^{\text{qudit}} = 3 \times 10^{-3}$ . This value is roughly one order of magnitude smaller than the two-qudit gate errors reported for qudit-based trapped-ion quantum computers [31, 33, 38]. Theoretically, it has been suggested that two-qudit gate errors smaller than  $10^{-2}$  can in principle be achieved by trapped-ion quantum computers [89].

## B. Three-mode model of H<sub>2</sub>O

In this section, we compare the qubit and qudit encodings for a model of H<sub>2</sub>O, including three vibrational modes: symmetric stretch ( $\nu_1$ ), bending ( $\nu_2$ ), and anti-symmetric stretch ( $\nu_3$ ). We employ the following values of the harmonic frequencies  $\omega_k$  and the anharmonic constants  $f_{jkl}$ , taken from [90]:

$$\begin{aligned} \omega_1 &= 3843.74 \text{ cm}^{-1}, \\ \omega_2 &= 1641.18 \text{ cm}^{-1}, \\ \omega_3 &= 3948.48 \text{ cm}^{-1}, \end{aligned} \quad (32)$$

and

$$\begin{aligned} f_{111} &= 303.64 \text{ cm}^{-1}, \\ f_{112} &= 39.02 \text{ cm}^{-1}, \\ f_{122} &= -162.13 \text{ cm}^{-1}, \\ f_{222} &= -43.96 \text{ cm}^{-1}, \\ f_{133} &= 911.05 \text{ cm}^{-1}, \\ f_{233} &= 134.59 \text{ cm}^{-1}. \end{aligned} \quad (33)$$

All other  $f_{jkl}$  equal 0.

### 1. Qubit and qudit Hamiltonians

In Fig. 3, we show the number of terms  $L_q$  in the qubit and qudit H<sub>2</sub>O Hamiltonians. Because of the larger number of modes,  $L_q$  is larger than for the two-mode CO<sub>2</sub> model,

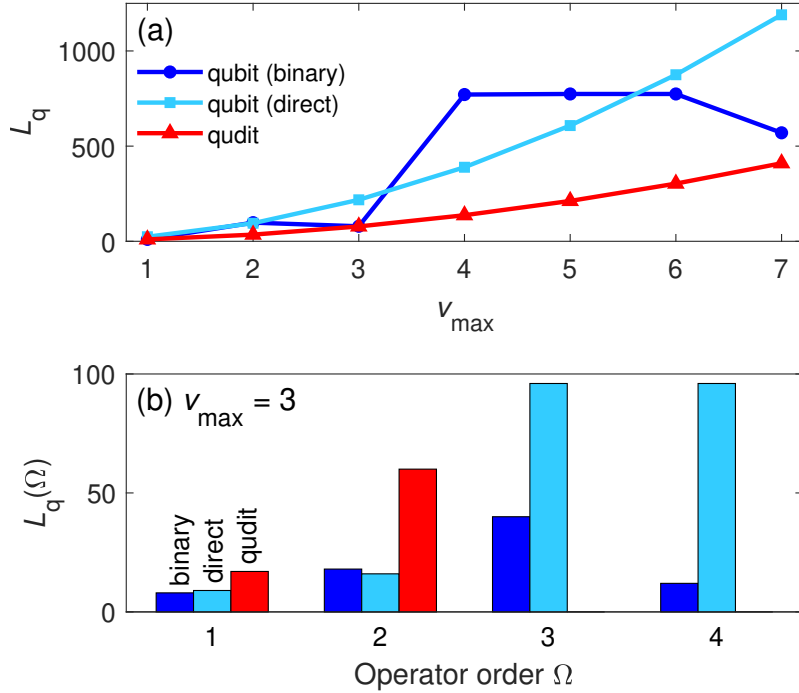


FIG. 3. (a) Number of terms  $L_q$  in the qubit/qudit Hamiltonian for the three-mode model of  $\text{H}_2\text{O}$ . (b) Number of terms  $L_q(\Omega)$  for each operator order  $\Omega$ , at  $v_{\max} = 3$ .

but shows the same behavior as a function of  $v_{\max}$  as in Fig. 1(a). The distribution of the number of terms as a function of the operator order shown in Fig. 3(b) is also similar to that of  $\text{CO}_2$ : The direct and binary qubit encodings result in qubit Hamiltonians containing three- and four-qubit operators, while the qudit Hamiltonian only contains one- and two-qudit operators. At  $v_{\max} = 3$ , the binary qubit encoding requires six qubits, the direct qubit encoding requires 12 qubits, and three qudits are used in the qudit encoding. The reason for the absence of three-qudit operators in the qudit Hamiltonian is that there are no three-mode interaction terms in the vibrational Hamiltonian [see Eq. (33)].

## 2. Time-dependent vibrational dynamics

In Fig. 4, we show time-dependent populations in  $\text{H}_2\text{O}$  for  $v_{\max} = 3$ , assuming that the initial state is  $|v_1, v_2, v_3\rangle = |2, 0, 0\rangle$ . Because the direct qubit encoding results in a large number of terms in the qubit Hamiltonian ( $L_q = 218$ ), we only compare the qubit binary encoding ( $L_q = 79$ ) and the qudit ( $d = 4$ ) encoding ( $L_q = 78$ ). We use a value of  $\epsilon_{2q} = 10^{-3}$  in the qubit as well as in the qudit simulations. The number of two-qubit gates in the

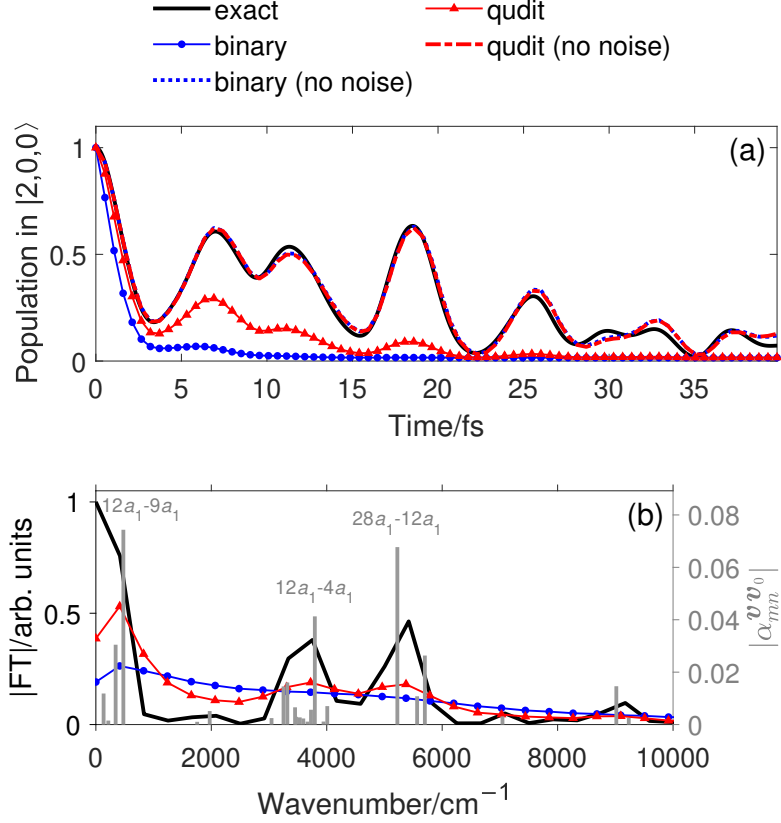


FIG. 4. (a) Time-dependent population  $p_{200}(t)$  in the  $|\mathbf{v}\rangle = |2,0,0\rangle$  state for  $\text{H}_2\text{O}$  with  $v_{\max} = 3$ . The initial state is  $|\mathbf{v}_0\rangle = |2,0,0\rangle$ , the Suzuki-Trotter step size is  $\Delta t = 0.53$  fs, and the two-qubit/qudit gate error is  $\epsilon_{2q} = 10^{-3}$ . (b) Normalized absolute value of the Fourier transform of the time-dependent populations in (a). The Fourier transform of the noiseless Suzuki-Trotter simulations are not shown. The horizontal positions of the gray sticks indicate the energy differences  $\Delta E_{mn} = E_m - E_n$  obtained by matrix diagonalization of  $H_q$ . The length of each gray stick (right-hand vertical axis) is determined by the absolute value of the expansion coefficients  $\alpha_{mn}^{vv_0}$  [see Eq. (21)]. The state labels of the dominant transitions (see Table I in Appendix A) are indicated above the respective stick.

circuit for one Suzuki-Trotter step at  $v_{\max} = 3$  becomes  $\Lambda_{2q}(\text{binary}) = 198$  compared to  $\Lambda_{2q}(\text{qudit}) = 60$  two-qudit gates in the qudit circuit. Even though  $L_q(\text{qudit}) \approx L_q(\text{binary})$ ,  $\Lambda_{2q}(\text{qudit})$  is much smaller than  $\Lambda_{2q}(\text{binary})$  because of the absence of three- and four qudit terms in the qudit Hamiltonian.

The error arising from the Suzuki-Trotter approximation is small, as can be seen by comparing the “no noise” and “exact” curves in Fig. 4(a). We have  $|p_{200}^{\text{no noise}}(t) - p_{200}^{\text{exact}}(t)| <$

0.06 for both qubit and qudit encodings in the time range  $0 \leq t \leq 40$  fs shown in Fig. 4(a). The curves obtained by the simulation including the noise model are strongly damped. We obtain  $\tau_{\text{binary}} \approx 2.7$  fs and  $\tau_{\text{qudit}} \approx 8.8$  fs for the decay times as defined in Eq. (30).

The Fourier spectrum of the time-dependent populations is plotted in Fig. 4(b). There are many frequency components contributing to the time-dependent populations, as can be seen by the large number of gray vertical sticks in Fig. 4(b). For reference, we list in Appendix A the eigenenergies of our H<sub>2</sub>O model ( $v_{\text{max}} = 3$ ) obtained by matrix diagonalization. Broad peaks can be seen around the main three groups of transitions at  $500 \text{ cm}^{-1}$ ,  $3800 \text{ cm}^{-1}$ , and  $5200 \text{ cm}^{-1}$  in the case of the exact and qudit simulations. No clear peaks can be seen in the Fourier spectrum obtained in the qubit simulation.

### 3. Time-dependent vibrational dynamics at small error rates

In view of the prospects of fault-tolerant quantum computing, it is interesting to consider smaller gate errors  $\epsilon_{2q}$  than what is realized in current quantum hardware. For example, in Quantinuum’s roadmap [91], a logical gate error between  $10^{-5}$  and  $10^{-10}$  is expected to be realized in 2029. In Fig. 5, we show a simulation of the time-dependent vibrational dynamics employing the same parameters as in Fig. 4, except for a smaller two-qubit/qudit gate error of  $\epsilon_{2q} = 10^{-5}$ . The decay times are two orders of magnitude longer,  $\tau_{\text{binary}} \approx 270$  fs and  $\tau_{\text{qudit}} \approx 880$  fs. As can be seen in Fig. 5(b), because of the increased resolution due to the long decay time, most of the peaks in the Fourier spectrum obtained by the noisy qudit simulation can now be resolved. In Figs. 5(a) and (b), the curves obtained using the Suzuki-Trotter approximation without noise are not shown to avoid cluttering the plots. As illustrated in the enlarged view in Fig. 5(c), the positions of the peaks obtained in the Suzuki-Trotter simulations are different from those obtained in the exact simulation because of the algorithmic error in the Suzuki-Trotter approximation [see Eq. (26)]. In order to increase the accuracy, a higher-order Suzuki-Trotter formula [92] needs to be used.

## IV. SUMMARY

We have simulated vibrational dynamics of two molecules, CO<sub>2</sub> and H<sub>2</sub>O, using qubit and qudit encodings, including the effect of noise. We showed that for both molecules, the qudit

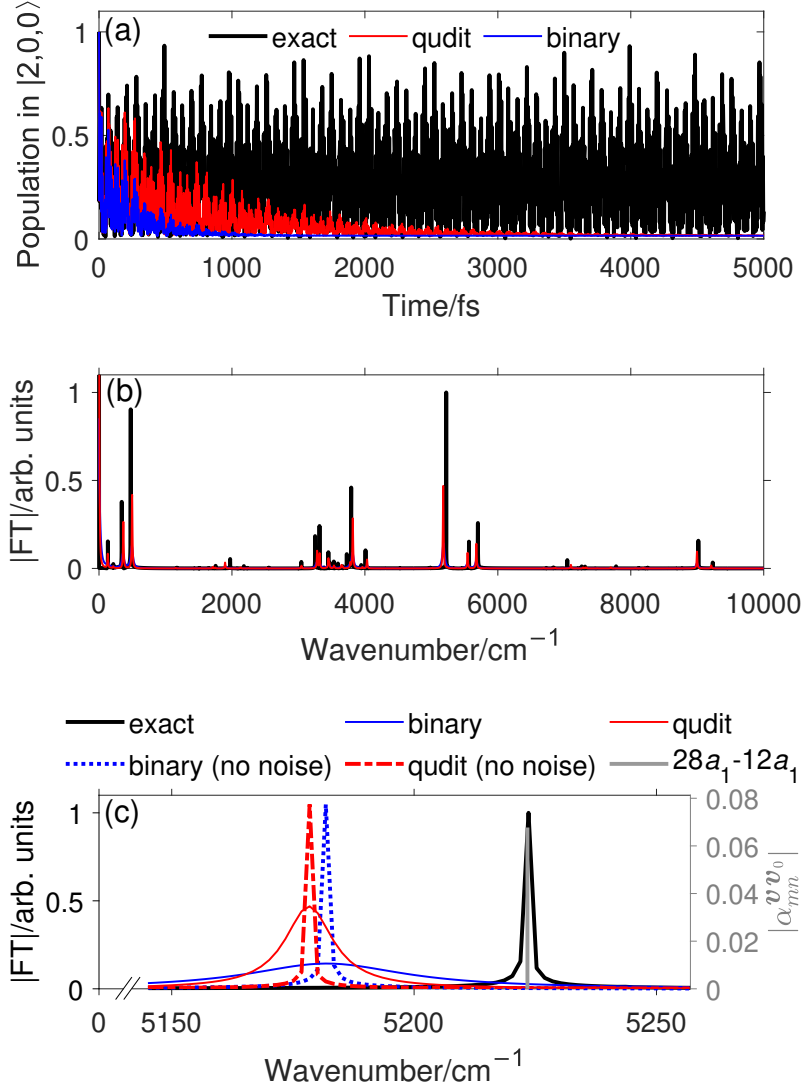


FIG. 5. (a) Time-dependent population  $p_{200}(t)$  in the  $|\mathbf{v}\rangle = |2, 0, 0\rangle$  state of  $\text{H}_2\text{O}$ . All parameters are the same as those employed in Fig. 4 ( $v_{\max} = 3$ ,  $|\mathbf{v}_0\rangle = |2, 0, 0\rangle$ ,  $\Delta t = 0.53$  fs), except the two-qubit/qudit gate error which is  $\epsilon_{2q} = 10^{-5}$ . (b) Normalized absolute value of the Fourier transform of the time-dependent populations in (a). In panels (a) and (b), the no-noise curves are not shown to avoid cluttering the plot. (c) Zoom-in of the Fourier spectra in (b) in the wavenumber range  $5150 \text{ cm}^{-1} \leq \tilde{\nu} \leq 5250 \text{ cm}^{-1}$ . The curves obtained without noise (but with the Suzuki-Trotter approximation) are also shown. The gray vertical stick indicates the exact energy difference  $E_{28a_1} - E_{12a_1} = 5223.4 \text{ cm}^{-1}$  obtained by matrix diagonalization of  $H_q$ . The length of the gray stick is given by  $|\alpha_{mn}^{vv_0}|$  [see Eq. (21)], with the numerical value shown on the right-hand vertical axis. The “binary” and “qudit” curves obtained with a noise model in (b) and (c) are multiplied by a factor of five to make the comparison with the other curves easier.

representation of the Hamiltonian is more compact than the qubit representation, and therefore, the simulations using the qudit encoding are more accurate than those using the qubit encodings resulting in the time-dependent populations closer to the populations obtained in the absence of noise. Our results show that simulation of vibrational dynamics is an interesting application of existing and future qudit quantum computers. We mention that similarly to the damped spin dynamics considered in [93, 94], damped vibrational dynamics simulated on noisy quantum computers may serve as a model for the simulation of vibrational energy relaxation in liquids [95, 96]. Once a gate error of  $\epsilon_{2q} \sim 10^{-5}$  or smaller is achieved, more accurate quantum computing of vibrational dynamics of polyatomic molecules becomes possible so that vibrational energy transfer and vibrational energy relaxation can be simulated.

## V. DATA AVAILABILITY

The data supporting the findings of this article are openly available at [86].

## ACKNOWLEDGMENTS

We thank T. Nishi (I-ALFA, The University of Tokyo) for helpful comments. We are supported by the JSPS (Kakenhi no. JP24K08336), the RIKEN TRIP initiative (RIKEN Quantum), and JST-CREST Quantum Frontiers (grant no. JPMJCR23I7). We are grateful to the DIC Corporation for their support through the Applied Quantum Chemistry by Qubits (AQUABIT) project under the UTokyo Quantum Initiative.

### Appendix A: Vibrational energy levels of H<sub>2</sub>O

In Table I, we show the vibrational energy levels of H<sub>2</sub>O with energy smaller than 13000 cm<sup>-1</sup>, obtained by diagonalization of  $H_q(v_{\max} = 3)$ . Because the symmetry of the  $\nu_1$  and  $\nu_2$  modes is  $A_1$  and that of the  $\nu_3$  mode is  $B_2$  in the  $C_{2v}$  point group, the symmetry of an eigenstate having even  $v_3$  is  $A_1$  and that of an eigenstate having odd  $v_3$  is  $B_2$ . The vibrational levels having symmetry  $A_1$  correspond to para-H<sub>2</sub>O (singlet proton spin state), and those having  $B_2$  symmetry correspond to ortho-H<sub>2</sub>O (triplet proton spin state).

For reference, we compare in Table II the energy difference  $\Delta E_n$  relative to the vibrational

TABLE I. Vibrational energy levels of H<sub>2</sub>O ( $v_{\max} = 3$ ), labeled by their symmetry species in the  $C_{2v}$  point group. In the last column, we list the dominant basis functions in the expansion (22) for expansion coefficients  $\psi_{\mathbf{v}n}^2 \geq 0.2$ .

$n$	Symmetry	$E_n/\text{cm}^{-1}$	$v_1 v_2 v_3 (\psi_{\mathbf{v}n}^2)$
0	$a_1$	-130.87	000(0.97)
1	$a_1$	1542.32	010(0.98)
2	$a_1$	3171.32	020(0.83)
3	$b_2$	3349.39	001(0.83)
4	$a_1$	3386.98	100(0.69)
5	$a_1$	4815.56	030(0.77)
6	$b_2$	5085.57	011(0.84)
7	$a_1$	5138.58	110(0.66), 030(0.22)
8	$b_2$	6489.93	101(0.46), 201(0.21)
9	$a_1$	6704.16	120(0.48)
10	$b_2$	6830.69	021(0.83)
11	$a_1$	6838.06	120(0.37), 002(0.28)
12	$a_1$	7180.56	200(0.44), 002(0.35)
13	$b_2$	8206.29	111(0.45)
14	$a_1$	8352.48	130(0.52), 210(0.23)
15	$b_2$	8576.36	031(0.78)
16	$a_1$	8608.96	012(0.33), 130(0.31)
17	$a_1$	8933.74	210(0.40), 012(0.37)
18	$b_2$	9987.84	121(0.52)
19	$b_2$	10207.94	003(0.32), 103(0.24), 101(0.21)
20	$a_1$	10224.16	220(0.41), 022(0.21)
21	$a_1$	10431.68	102(0.30), 202(0.27)
22	$a_1$	10648.78	022(0.55), 220(0.25)
23	$b_2$	10721.64	201(0.37), 003(0.28)
24	$b_2$	11687.50	131(0.52)
25	$a_1$	11915.24	230(0.45)
26	$b_2$	11994.01	013(0.26)
27	$a_1$	12165.94	112(0.27), 212(0.21)
28	$a_1$	12403.94	300(0.79)
29	$a_1$	12424.51	032(0.56)
30	$b_2$	12449.26	013(0.35), 211(0.34)

ground state, defined as

$$\Delta E_n = E_n - E_0, \quad (\text{A1})$$

with the experimentally measured energy differences [97] for the four lowest excited states. As can be seen in Table II, the energy differences obtained using the H<sub>2</sub>O model defined by Eqs. (32) and (33) differ by more than 100 cm<sup>-1</sup> from the experimentally measured energy differences. The main reason for the discrepancy is the omission of fourth-order terms in

TABLE II. Excitation energies  $\Delta E_n$  in  $\text{cm}^{-1}$  of the lowest four excited vibrational states of  $\text{H}_2\text{O}$  ( $v_{\text{max}} = 3$ ). Each column is labeled by  $n\gamma(v_1v_2v_3)$ , where  $n$  is the state number from Table I,  $\gamma$  is the symmetry species, and  $v_1v_2v_3$  is the dominant basis function. We also show the experimentally measured energies differences in the rotational ground state whose total angular momentum is  $J = 0$ .

	$1a_1(010)$	$2a_1(020)$	$3b_2(001)$	$4a_1(100)$
H <sub>2</sub> O model	1673.20	3302.19	3480.27	3517.85
Exp. <sup>a</sup>	1594.75	3151.63	3755.93	3657.05

<sup>a</sup> W2020 database [97].

the anharmonic potential (33).

## REFERENCES

- [1] S. Bravyi, O. Dial, J. M. Gambetta, D. Gil, and Z. Nazario, “The future of quantum computing with superconducting qubits,” *J. Appl. Phys.* **132**, 160902 (2022).
- [2] S. A. Moses, C. H. Baldwin, M. S. Allman, R. Ancona, L. Ascarrunz, C. Barnes, J. Bartolotta, B. Bjork, P. Blanchard, M. Bohn, J. G. Bohnet, N. C. Brown, N. Q. Burdick, W. C. Burton, S. L. Campbell, J. P. Campora, C. Carron, J. Chambers, J. W. Chan, Y. H. Chen, A. Chernoguzov, E. Chertkov, J. Colina, J. P. Curtis, R. Daniel, M. DeCross, D. Deen, C. Delaney, J. M. Dreiling, C. T. Ertsgaard, J. Esposito, B. Estey, M. Fabrikant, C. Figgatt, C. Foltz, M. Foss-Feig, D. Francois, J. P. Gaebler, T. M. Gatterman, C. N. Gilbreth, J. Giles, E. Glynn, A. Hall, A. M. Hankin, A. Hansen, D. Hayes, B. Higashi, I. M. Hoffman, B. Horning, J. J. Hout, R. Jacobs, J. Johansen, L. Jones, J. Karcz, T. Klein, P. Lauria, P. Lee, D. Liefer, S. T. Lu, D. Lucchetti, C. Lytle, A. Malm, M. Matheny, B. Mathewson, K. Mayer, D. B. Miller, M. Mills, B. Neyenhuis, L. Nugent, S. Olson, J. Parks, G. N. Price, Z. Price, M. Pugh, A. Ransford, A. P. Reed, C. Roman, M. Rowe, C. Ryan-Anderson, S. Sanders, J. Sedlacek, P. Shevchuk, P. Siegfried, T. Skripka, B. Spaun, R. T. Sprenkle, R. P. Stutz, M. Swallows, R. I. Tobey, A. Tran, T. Tran, E. Vogt, C. Volin, J. Walker, A. M. Zolot, and J. M. Pino, “A race-track trapped-ion quantum processor,” *Phys. Rev. X* **13**, 041052 (2023).
- [3] J.-S. Chen, E. Nielsen, M. Ebert, V. Inlek, K. Wright, V. Chaplin, A. Maksymov, E. Páez, A. Poudel, P. Maunz, and J. Gamble, “Benchmarking a trapped-ion quantum computer with 30 qubits,” *Quantum* **8**, 1516 (2024).
- [4] Y. Chew, T. Tomita, T. P. Mahesh, S. Sugawa, S. de Léséleuc, and K. Ohmori, “Ultrafast energy exchange between two single Rydberg atoms on a nanosecond timescale,” *Nature Photonics* **16**, 724 (2022).
- [5] D. Bluvstein, S. J. Evered, A. A. Geim, S. H. Li, H. Zhou, T. Manovitz, S. Ebadi, M. Cain, M. Kalinowski, D. Hangleiter, J. P. B. Ataiades, N. Maskara, I. Cong, X. Gao, P. S. Rodriguez, T. Karolyshyn, G. Semeghini, M. J. Gullans, M. Greiner, V. Vuletić, and M. D. Lukin, “Logical quantum processor based on reconfigurable atom arrays,” *Nature* **626**, 58 (2024).
- [6] X.-Q. Shao, S.-L. Su, L. Li, R. Nath, J.-H. Wu, and W. Li, “Rydberg superatoms: An artificial quantum system for quantum information processing and quantum optics,” *Appl. Phys. Rev.* **11**, 031320 (2024).

- [7] IBM Quantum Platform, <https://quantum.cloud.ibm.com/>.
- [8] A. Ransford, M. S. Allman, J. Arkininstall, J. P. Campora, S. F. Cooper, R. D. Delaney, J. M. Dreiling, B. Estey, C. Figgatt, A. Hall, A. A. Husain, A. Isanaka, C. J. Kennedy, N. Kotibhaskar, I. S. Madjarov, K. Mayer, A. R. Milne, A. J. Park, A. P. Reed, R. Ancona, M. P. Andersen, P. Andres-Martinez, W. Angenent, L. Argueta, B. Arkin, L. Ascarrunz, W. Baker, C. Barnes, J. Bartolotta, J. Berg, R. Besand, B. Bjork, M. Blain, P. Blanchard, R. Blume-Kohout, M. Bohn, A. Borgna, D. Y. Botamanenko, R. Boutelle, N. Brown, G. T. Buckingham, N. Q. Burdick, W. C. Burton, V. Carey, C. J. Carron, J. Chambers, J. Children, V. E. Colussi, S. Crepinsek, A. Cureton, J. Davies, D. Davis, M. DeCross, D. Deen, C. Delaney, D. DelVento, B. J. DeSalvo, J. Dominy, R. Duncan, V. Eccles, A. Edgington, N. Erickson, S. Erickson, C. T. Ertsgaard, B. Evans, T. Evans, M. I. Fabrikant, A. Fischer, C. Foltz, M. Foss-Feig, D. Francois, B. Freyberg, C. Gao, R. Garay, J. Garvin, D. M. Gaudiosi, C. N. Gilbreth, J. Giles, E. Glynn, J. Graves, A. Hansen, D. Hayes, L. Heidemann, B. Higashi, T. Hilbun, J. Hines, A. Hlavaty, K. Hoffman, I. M. Hoffman, C. Holliman, I. Hooper, B. Horning, J. Hostetter, D. Hothem, J. Houlton, J. Hout, R. Hutson, R. T. Jacobs, T. Jacobs, M. Johannsen, J. Johansen, L. Jones, S. Julian, R. Jung, A. Keay, T. Klein, M. Koch, R. Kondo, C. Kong, A. Kosto, A. Lawrence, D. Liefer, M. Lollie, D. Lucchetti, N. K. Lysne, C. Lytle, C. MacPherson, A. Malm, S. Mather, B. Mathewson, D. Maxwell, L. McCaffrey, H. McDougall, R. Mendoza, M. Mills, R. Morrison, L. Narmour, N. Nguyen, L. Nugent, S. Olson, D. Ouellette, J. Parks, Z. Peters, J. Petricka, J. M. Pino, F. Polito, M. Preidl, G. Price, T. Proctor, M. Pugh, N. Ratcliff, D. Raymondson, P. Rhodes, C. Roman, C. Roy, C. Ryan-Anderson, F. B. Sanchez, G. Sangiolo, T. Sawadski, A. Schaffer, P. Schow, J. Sedlacek, H. Semenenko, P. Shevchuk, S. Shore, P. Siegfried, K. Singhal, S. Sivarajah, T. Skripka, L. Sletten, B. Spaun, R. T. Sprenkle, P. Stoufer, M. Tader, S. F. Taylor, T. H. Thompson, R. Tobey, A. Tran, T. Tran, G. Vittorini, C. Volin, J. Walker, S. White, D. Wilson, Q. Wolf, C. Wringe, K. Young, J. Zheng, K. Zuraski, C. H. Baldwin, A. Chernoguzov, J. P. Gaebler, S. J. Sanders, B. Neyenhuis, R. Stutz, and J. G. Bohnet, “Helios: A 98-qubit trapped-ion quantum computer,” (2025), arXiv:2511.05465 [quant-ph].
- [9] Y. Cao, J. Romero, J. P. Olson, M. Degroote, P. D. Johnson, M. Kieferová, I. D. Kivlichan, T. Menke, B. Peropadre, N. P. D. Sawaya, S. Sim, L. Veis, and A. Aspuru-Guzik, “Quantum chemistry in the age of quantum computing,” *Chem. Rev.* **119**, 10856 (2019).
- [10] B. Bauer, S. Bravyi, M. Motta, and G. K.-L. Chan, “Quantum algorithms for quantum

- chemistry and quantum materials science,” *Chem. Rev.* **120**, 12685 (2020).
- [11] S. McArdle, S. Endo, A. Aspuru-Guzik, S. C. Benjamin, and X. Yuan, “Quantum computational chemistry,” *Rev. Mod. Phys.* **92**, 015003 (2020).
- [12] J. D. Weidman, M. Sajjan, C. Mikolas, Z. J. Stewart, J. Pollanen, S. Kais, and A. K. Wilson, “Quantum computing and chemistry,” *Cell Rep. Phys. Sci.* **5**, 102105 (2024).
- [13] A. Eddins, M. Motta, T. P. Gujarati, S. Bravyi, A. Mezzacapo, C. Hadfield, and S. Sheldon, “Doubling the size of quantum simulators by entanglement forging,” *PRX Quantum* **3**, 010309 (2022).
- [14] S. Guo, J. Sun, H. Qian, M. Gong, Y. Zhang, F. Chen, Y. Ye, Y. Wu, S. Cao, K. Liu, C. Zha, C. Ying, Q. Zhu, H.-L. Huang, Y. Zhao, S. Li, S. Wang, J. Yu, D. Fan, D. Wu, H. Su, H. Deng, H. Rong, Y. Li, K. Zhang, T.-H. Chung, F. Liang, J. Lin, Y. Xu, L. Sun, C. Guo, N. Li, Y.-H. Huo, C.-Z. Peng, C.-Y. Lu, X. Yuan, X. Zhu, and J.-W. Pan, “Experimental quantum computational chemistry with optimized unitary coupled cluster ansatz,” *Nat. Phys.* **20**, 1240 (2024).
- [15] A. Tranter, P. J. Love, F. Mintert, and P. V. Coveney, “A comparison of the Bravyi-Kitaev and Jordan-Wigner transformations for the quantum simulation of quantum chemistry,” *J. Chem. Theory Comput.* **14**, 5617 (2018).
- [16] Y. Alexeev, M. Amsler, M. A. Barroca, S. Bassini, T. Battelle, D. Camps, D. Casanova, Y. J. Choi, F. T. Chong, C. Chung, C. Codella, A. D. Córcoles, J. Cruise, A. Di Meglio, I. Duran, T. Eckl, S. Economou, S. Eidenbenz, B. Elmgreen, C. Fare, I. Faro, C. S. Fernández, R. N. B. Ferreira, K. Fuji, B. Fuller, L. Gagliardi, G. Galli, J. R. Glick, I. Gobbi, P. Gokhale, S. de la Puente Gonzalez, J. Greiner, B. Gropp, M. Grossi, E. Gull, B. Healy, M. R. Hermes, B. Huang, T. S. Humble, N. Ito, A. F. Izmaylov, A. Javadi-Abhari, D. Jennewein, S. Jha, L. Jiang, B. Jones, W. A. de Jong, P. Jurcevic, W. Kirby, S. Kister, M. Kitagawa, J. Klassen, K. Klymko, K. Koh, M. Kondo, D. M. Kürkçüoğlu, K. Kurowski, T. Laino, R. Landfield, M. Leininger, V. Leyton-Ortega, A. Li, M. Lin, J. Liu, N. Lorente, A. Luckow, S. Martiel, F. Martin-Fernandez, M. Martonosi, C. Marvinney, A. C. Medina, D. Merten, A. Mezzacapo, K. Michielsen, A. Mitra, T. Mittal, K. Moon, J. Moore, S. Mostame, M. Motta, Y.-H. Na, Y. Nam, P. Narang, Y.-y. Ohnishi, D. Ottaviani, M. Otten, S. Pakin, V. R. Pascuzzi, E. Pednault, T. Piontek, J. Pitera, P. Rall, G. S. Ravi, N. Robertson, M. A. Rossi, P. Rydlichowski, H. Ryu, G. Samsonidze, M. Sato, N. Saurabh, V. Sharma, K. Sharma, S. Shin, G. Slessman,

- M. Steiner, I. Sitdikov, I.-S. Suh, E. D. Switzer, W. Tang, J. Thompson, S. Todo, M. C. Tran, D. Tenev, C. Trott, H.-H. Tseng, N. M. Tubman, E. Tureci, D. G. Valiñas, S. Vallecorsa, C. Wever, K. Wojciechowski, X. Wu, S. Yoo, N. Yoshioka, V. W.-z. Yu, S. Yunoki, S. Zhuk, and D. Zubarev, “Quantum-centric supercomputing for materials science: A perspective on challenges and future directions,” *Future Gener. Comput. Syst.* **160**, 666 (2024).
- [17] K. Kanno, M. Kohda, R. Imai, S. Koh, K. Mitarai, W. Mizukami, and Y. O. Nakagawa, “Quantum-selected configuration interaction: classical diagonalization of Hamiltonians in subspaces selected by quantum computers,” (2023), arXiv:2302.11320 [quant-ph].
- [18] Y. O. Nakagawa, M. Kamoshita, W. Mizukami, S. Sudo, and Y.-y. Ohnishi, “ADAPT-QSCI: Adaptive construction of an input state for quantum-selected configuration interaction,” *J. Chem. Theory Comput.* **20**, 10817 (2024).
- [19] J. Robledo-Moreno, M. Motta, H. Haas, A. Javadi-Abhari, P. Jurcevic, W. Kirby, S. Martiel, K. Sharma, S. Sharma, T. Shirakawa, I. Sitdikov, R.-Y. Sun, K. J. Sung, M. Takita, M. C. Tran, S. Yunoki, and A. Mezzacapo, “Chemistry beyond the scale of exact diagonalization on a quantum-centric supercomputer,” *Science Advances* **11**, eadu9991 (2025).
- [20] A. Muthukrishnan and C. R. Stroud, “Multivalued logic gates for quantum computation,” *Phys. Rev. A* **62**, 052309 (2000).
- [21] A. Y. Vlasov, “Noncommutative tori and universal sets of nonbinary quantum gates,” *J. Math. Phys.* **43**, 2959 (2002).
- [22] Y. Wang, Z. Hu, B. C. Sanders, and S. Kais, “Qudits and high-dimensional quantum computing,” *Front. Phys.* **8**, 589504 (2020).
- [23] R. Bianchetti, S. Filipp, M. Baur, J. M. Fink, C. Lang, L. Steffen, M. Boissonneault, A. Blais, and A. Wallraff, “Control and tomography of a three level superconducting artificial atom,” *Phys. Rev. Lett.* **105**, 223601 (2010).
- [24] M. S. Blok, V. V. Ramasesh, T. Schuster, K. O’Brien, J. M. Kreikebaum, D. Dahlen, A. Morvan, B. Yoshida, N. Y. Yao, and I. Siddiqi, “Quantum information scrambling on a superconducting qutrit processor,” *Phys. Rev. X* **11**, 021010 (2021).
- [25] K. Luo, W. Huang, Z. Tao, L. Zhang, Y. Zhou, J. Chu, W. Liu, B. Wang, J. Cui, S. Liu, F. Yan, M.-H. Yung, Y. Chen, T. Yan, and D. Yu, “Experimental realization of two qutrits gate with tunable coupling in superconducting circuits,” *Phys. Rev. Lett.* **130**, 030603 (2023).
- [26] T. Roy, Z. Li, E. Kapit, and D. Schuster, “Two-qutrit quantum algorithms on a programmable

- superconducting processor,” *Phys. Rev. Appl.* **19**, 064024 (2023).
- [27] N. Goss, S. Ferracin, A. Hashim, A. Carignan-Dugas, J. M. Kreikebaum, R. K. Naik, D. I. Santiago, and I. Siddiqi, “Extending the computational reach of a superconducting qutrit processor,” *npj Quantum Inf.* **10**, 101 (2024).
- [28] Z. Wang, R. W. Parker, E. Champion, and M. S. Blok, “High- $E_J/E_C$  transmon qudits with up to 12 levels,” *Phys. Rev. Appl.* **23**, 034046 (2025).
- [29] J. Randall, S. Weidt, E. D. Standing, K. Lake, S. C. Webster, D. F. Murgia, T. Navickas, K. Roth, and W. K. Hensinger, “Efficient preparation and detection of microwave dressed-state qubits and qutrits with trapped ions,” *Phys. Rev. A* **91**, 012322 (2015).
- [30] C. Senko, P. Richerme, J. Smith, A. Lee, I. Cohen, A. Retzker, and C. Monroe, “Realization of a quantum integer-spin chain with controllable interactions,” *Phys. Rev. X* **5**, 021026 (2015).
- [31] M. Ringbauer, M. Meth, L. Postler, R. Stricker, R. Blatt, P. Schindler, and T. Monz, “A universal qudit quantum processor with trapped ions,” *Nat. Phys.* **18**, 1053 (2022).
- [32] M. A. Aksenov, I. V. Zalivako, I. A. Semerikov, A. S. Borisenko, N. V. Semenin, P. L. Sidorov, A. K. Fedorov, K. Y. Khabarova, and N. N. Kolachevsky, “Realizing quantum gates with optically addressable  $^{171}\text{Yb}^+$  ion qudits,” *Phys. Rev. A* **107**, 052612 (2023).
- [33] P. Hrmo, B. Wilhelm, L. Gerster, M. W. van Mourik, M. Huber, R. Blatt, P. Schindler, T. Monz, and M. Ringbauer, “Native qudit entanglement in a trapped ion quantum processor,” *Nat. Commun.* **14**, 2242 (2023).
- [34] C. Edmunds, E. Rico, I. Arrazola, G. Brennen, M. Meth, R. Blatt, and M. Ringbauer, “Symmetry-protected topological Haldane phase on a qudit quantum processor,” *PRX Quantum* **6**, 020349 (2025).
- [35] A. S. Nikolaeva, E. O. Kiktenko, and A. K. Fedorov, “Universal quantum computing with qubits embedded in trapped-ion qudits,” *Phys. Rev. A* **109**, 022615 (2024).
- [36] M. Meth, J. Zhang, J. F. Haase, C. Edmunds, L. Postler, A. J. Jena, A. Steiner, L. Dellantonio, R. Blatt, P. Zoller, T. Monz, P. Schindler, C. Muschik, and M. Ringbauer, “Simulating two-dimensional lattice gauge theories on a qudit quantum computer,” *Nat. Phys.* **21**, 570 (2025).
- [37] P. J. Low, B. White, and C. Senko, “Control and readout of a 13-level trapped ion qudit,” *npj Quantum Information* **11**, 85 (2025).
- [38] I. V. Zalivako, A. S. Nikolaeva, A. S. Borisenko, A. E. Korolkov, P. L. Sidorov, K. P. Galstyan, N. V. Semenin, V. N. Smirnov, M. A. Aksenov, K. M. Makushin, E. O. Kiktenko, A. K.

- Fedorov, I. A. Semerikov, K. Y. Khabarova, and N. N. Kolachevsky, “Towards a multi-qudit quantum processor based on a  $^{171}\text{Yb}^+$  ion string: Realizing basic quantum algorithms,” *Quantum Rep.* **7**, 19 (2025).
- [39] B. P. Lanyon, T. J. Weinhold, N. K. Langford, J. L. O’Brien, K. J. Resch, A. Gilchrist, and A. G. White, “Manipulating biphotonic qutrits,” *Phys. Rev. Lett.* **100**, 060504 (2008).
- [40] B. P. Lanyon, M. Barbieri, M. P. Almeida, T. Jennewein, T. C. Ralph, K. J. Resch, G. J. Pryde, J. L. O’Brien, A. Gilchrist, and A. G. White, “Simplifying quantum logic using higher-dimensional Hilbert spaces,” *Nat. Phys.* **5**, 134 (2009).
- [41] Y. Chi, J. Huang, Z. Zhang, J. Mao, Z. Zhou, X. Chen, C. Zhai, J. Bao, T. Dai, H. Yuan, M. Zhang, D. Dai, B. Tang, Y. Yang, Z. Li, Y. Ding, L. K. Oxenløwe, M. G. Thompson, J. L. O’Brien, Y. Li, Q. Gong, and J. Wang, “A programmable qudit-based quantum processor,” *Nat. Commun.* **13**, 1166 (2022).
- [42] I. Fernández de Fuentes, T. Botzem, M. A. I. Johnson, A. Vaartjes, S. Asaad, V. Mourik, F. E. Hudson, K. M. Itoh, B. C. Johnson, A. M. Jakob, J. C. McCallum, D. N. Jamieson, A. S. Dzurak, and A. Morello, “Navigating the 16-dimensional Hilbert space of a high-spin donor qudit with electric and magnetic fields,” *Nat. Commun.* **15**, 1380 (2024).
- [43] S. Chaudhury, S. Merkel, T. Herr, A. Silberfarb, I. H. Deutsch, and P. S. Jessen, “Quantum control of the hyperfine spin of a Cs atom ensemble,” *Phys. Rev. Lett.* **99**, 163002 (2007).
- [44] S. Omanakuttan, A. Mitra, M. J. Martin, and I. H. Deutsch, “Quantum optimal control of ten-level nuclear spin qudits in  $^{87}\text{Sr}$ ,” *Phys. Rev. A* **104**, 1060401 (2021).
- [45] J. Lindon, A. Tashchilina, L. W. Cooke, and L. J. LeBlanc, “Complete unitary qutrit control in ultracold atoms,” *Phys. Rev. Appl.* **19**, 034089 (2023).
- [46] V. A. Soltamov, C. Kasper, A. V. Poshakinskiy, A. N. Anisimov, E. N. Mokhov, A. Sperlich, S. A. Tarasenko, P. G. Baranov, G. V. Astakhov, and V. Dyakonov, “Excitation and coherent control of spin qudit modes in silicon carbide at room temperature,” *Nat. Commun.* **10**, 1678 (2019).
- [47] C. Adambukulam, B. C. Johnson, A. Morello, and A. Laucht, “Hyperfine spectroscopy and fast, all-optical arbitrary state initialization and readout of a single, ten-level  $^{73}\text{Ge}$  vacancy nuclear spin qudit in diamond,” *Phys. Rev. Lett.* **132**, 060603 (2024).
- [48] M. Chizzini, F. Tacchino, A. Chiesa, I. Tavernelli, S. Carretta, and P. Santini, “Qudit-based quantum simulation of fermionic systems,” *Phys. Rev. A* **110**, 062602 (2024).

- [49] R. J. MacDonell, C. E. Dickerson, C. J. T. Birch, A. Kumar, C. L. Edmunds, M. J. Biercuk, C. Hempel, and I. Kassal, “Analog quantum simulation of chemical dynamics,” *Chem. Sci.* **12**, 9794 (2021).
- [50] E. O. Kiktenko, A. S. Nikolaeva, and A. K. Fedorov, “Colloquium: Qudits for decomposing multiqubit gates and realizing quantum algorithms,” *Rev. Mod. Phys.* **97**, 021003 (2025).
- [51] A. S. Nikolaeva, E. O. Kiktenko, and A. K. Fedorov, “Generalized Toffoli gate decomposition using ququints: Towards realizing Grover’s algorithm with qudits,” *Entropy* **25**, 387 (2023).
- [52] A. S. Nikolaeva, E. O. Kiktenko, and A. K. Fedorov, “Efficient realization of quantum algorithms with qudits,” *EPJ Quantum Technol.* **11**, 43 (2024).
- [53] D. Gottesman, “Fault-tolerant quantum computation with higher-dimensional systems,” *Chaos Solit. Fractals* **10**, 1749 (1999).
- [54] E. T. Campbell, “Enhanced fault-tolerant quantum computing in  $d$ -level systems,” *Phys. Rev. Lett.* **113**, 230501 (2014).
- [55] J. Keppens, Q. Eggerickx, V. Levajac, G. Simion, and B. Sorée, “Qudit vs. qubit: Simulated performance of error-correction codes in higher dimensions,” *Phys. Rev. A* **112**, 032435 (2025).
- [56] D. Gottesman, A. Kitaev, and J. Preskill, “Encoding a qubit in an oscillator,” *Phys. Rev. A* **64**, 012310 (2001).
- [57] B. L. Brock, S. Singh, A. Eickbusch, V. V. Sivak, A. Z. Ding, L. Frunzio, S. M. Girvin, and M. H. Devoret, “Quantum error correction of qudits beyond break-even,” *Nature* **641**, 612 (2025).
- [58] A. Teplukhin, B. K. Kendrick, and D. Babikov, “Calculation of molecular vibrational spectra on a quantum annealer,” *J. Chem. Theory Comput.* **15**, 4555 (2019).
- [59] S. McArdle, A. Mayorov, X. Shan, S. Benjamin, and X. Yuan, “Digital quantum simulation of molecular vibrations,” *Chem. Sci.* **10**, 5725 (2019).
- [60] N. P. D. Sawaya and J. Huh, “Quantum algorithm for calculating molecular vibronic spectra,” *J. Phys. Chem. Lett.* **10**, 3586 (2019).
- [61] E. Lötstedt, K. Yamanouchi, T. Tsuchiya, and Y. Tachikawa, “Calculation of vibrational eigenenergies on a quantum computer: Application to the Fermi resonance in CO<sub>2</sub>,” *Phys. Rev. A* **103**, 062609 (2021).
- [62] E. Lötstedt, K. Yamanouchi, and Y. Tachikawa, “Evaluation of vibrational energies and wave functions of CO<sub>2</sub> on a quantum computer,” *AVS Quantum Science* **4**, 036801 (2022).

- [63] N. P. D. Sawaya, F. Paesani, and D. P. Tabor, “Near- and long-term quantum algorithmic approaches for vibrational spectroscopy,” *Phys. Rev. A* **104**, 062419 (2021).
- [64] M. Majland, R. Berg Jensen, M. G. Højlund, N. Thomas Zinner, and O. Christiansen, “Optimizing the number of measurements for vibrational structure on quantum computers: coordinates and measurement schemes,” *Chem. Sci.* **14**, 7733 (2023).
- [65] R. Somasundaram, R. Jayaharish, R. Ramanan, and C. Chowdhury, “Quantum computing for molecular vibrational energies: A comprehensive study,” *Mater. Today Quantum* **6**, 100031 (2025).
- [66] E. Lötstedt and T. Szidarovszky, “Rovibrational energy levels of H<sub>2</sub>O by quantum computing,” (2026), arXiv:2603.05795 [quant-ph].
- [67] K. Asnaashari, D. Bondarenko, and R. V. Krems, “Advantages of discrete variable representation in variational quantum eigensolvers for vibrational energy calculations,” *Phys. Chem. Chem. Phys.* **28**, 7900 (2026).
- [68] P. J. Ollitrault, A. Baiardi, M. Reiher, and I. Tavernelli, “Hardware efficient quantum algorithms for vibrational structure calculations,” *Chem. Sci.* **11**, 6842 (2020).
- [69] A. G. Császár, “Anharmonic molecular force fields,” *WIREs Comput. Mol. Sci.* **2**, 273 (2011).
- [70] N. P. D. Sawaya, T. Menke, T. H. Kyaw, S. Johri, A. Aspuru-Guzik, and G. G. Guerreschi, “Resource-efficient digital quantum simulation of  $d$ -level systems for photonic, vibrational, and spin- $s$  Hamiltonians,” *npj Quantum Inf.* **6**, 49 (2020).
- [71] S. Hadfield, Z. Wang, B. O’Gorman, E. G. Rieffel, D. Venturelli, and R. Biswas, “From the quantum approximate optimization algorithm to a quantum alternating operator ansatz,” *Algorithms* **12**, 34 (2019).
- [72] M.-X. Luo, X.-B. Chen, Y.-X. Yang, and X. Wang, “Geometry of quantum computation with qudits,” *Sci. Rep.* **4**, 4044 (2014).
- [73] E. Lötstedt and K. Yamanouchi, “Comparison of encoding schemes for quantum computing of  $S > 1/2$  spin chains,” *Phys. Rev. A* **111**, 062416 (2025).
- [74] H. F. Trotter, “On the product of semi-groups of operators,” *Proc. Amer. Math. Soc.* **10**, 545 (1959).
- [75] M. Suzuki, “Generalized Trotter’s formula and systematic approximants of exponential operators and inner derivations with applications to many-body problems,” *Commun. Math. Phys.* **51**, 183 (1976).

- [76] M. A. Nielsen and I. L. Chuang, *Quantum Computation and Quantum Information* (Cambridge University Press, Cambridge, UK, 2010).
- [77] P. V. Sriluckshmy, V. Pina-Canelles, M. Ponce, M. G. Algaba, F. Šimkovic IV, and M. Leib, “Optimal, hardware native decomposition of parameterized multi-qubit Pauli gates,” *Quantum Sci. Technol.* **8**, 045029 (2023).
- [78] M. B. Hastings, D. Wecker, B. Bauer, and M. Troyer, “Improving quantum algorithms for quantum chemistry,” *Quantum Info. Comput.* **15**, 1 (2015).
- [79] D. Poulin, M. B. Hastings, D. Wecker, N. Wiebe, A. C. Doberty, and M. Troyer, “The Trotter step size required for accurate quantum simulation of quantum chemistry,” *Quantum Info. Comput.* **15**, 361 (2015).
- [80] A. Tranter, P. J. Love, F. Mintert, N. Wiebe, and P. V. Coveney, “Ordering of Trotterization: Impact on errors in quantum simulation of electronic structure,” *Entropy* **21**, 1218 (2019).
- [81] I. Suzuki, “General anharmonic force constants of carbon dioxide,” *J. Mol. Spectroscopy* **25**, 479 (1968).
- [82] E. Fermi, “Über den Ramaneffekt des Kohlendioxyds,” *Z. Physik* **71**, 250 (1931).
- [83] V. Rodriguez-Garcia, S. Hirata, K. Yagi, K. Hirao, T. Taketsugu, I. Schweigert, and M. Tasumi, “Fermi resonance in CO<sub>2</sub>: A combined electronic coupled-cluster and vibrational configuration-interaction prediction,” *J. Chem. Phys.* **126**, 124303 (2007).
- [84] S. Sivarajah, S. Dilkes, A. Cowtan, W. Simmons, A. Edgington, and R. Duncan, “t|ket): a retargetable compiler for NISQ devices,” *Quantum Sci. Technol.* **6**, 014003 (2020).
- [85] D. Kremer, V. Villar, H. Paik, I. Duran, I. Faro, and J. Cruz-Benito, “Practical and efficient quantum circuit synthesis and transpiling with reinforcement learning,” (2024), arXiv:2405.13196 [quant-ph].
- [86] E. Lötstedt and K. Yamanouchi, “Simulation of vibrational dynamics using qubits and qudits,” Zenodo dataset (2026), doi:10.5281/zenodo.20115329.
- [87] T. Ando, A. Iwasaki, and K. Yamanouchi, “Strong-field Fourier transform vibrational spectroscopy of D<sub>2</sub><sup>+</sup> using few-cycle near-infrared laser pulses,” *Phys. Rev. Lett.* **120**, 263002 (2018).
- [88] T. Ando, K. Yamada, A. Iwasaki, and K. Yamanouchi, “Isotope shift of fine structure of Kr<sup>+</sup> and hyperfine structure of <sup>83</sup>Kr<sup>+</sup> by strong-field ultrahigh-resolution Fourier-transform spectroscopy,” *Phys. Rev. Res.* **7**, 1022025 (2025).
- [89] P. J. Low, B. M. White, A. A. Cox, M. L. Day, and C. Senko, “Practical trapped-ion protocols

- for universal qudit-based quantum computing,” *Phys. Rev. Res.* **2**, 033128 (2020).
- [90] A. G. Császár and I. M. Mills, “Vibrational energy levels of water,” *Spectrochim. Acta. A* **53**, 1101 (1997).
- [91] Quantinuum, “Quantinuum roadmap,” <https://www.quantinuum.com/press-releases/quantinuum-unveils-accelerated-roadmap-to-achieve-universal-fault-tolerant-quantum-computing-by-2030> (2024), accessed on April 2, 2026.
- [92] J. Ostmeier, “Optimised Trotter decompositions for classical and quantum computing,” *J. Phys. A: Math. Theor.* **56**, 285303 (2023).
- [93] B. Rost, B. Jones, M. Vyushkova, A. Ali, C. Cullip, A. Vyushkov, and J. Nabrzyski, “Simulation of thermal relaxation in spin chemistry systems on a quantum computer using inherent qubit decoherence,” (2020), arXiv:2001.00794 [quant-ph].
- [94] J. Leppäkangas, N. Vogt, K. R. Fratus, K. Bark, J. A. Vaitkus, P. Stadler, J.-M. Reiner, S. Zanker, and M. Marthaler, “Quantum algorithm for solving open-system dynamics on quantum computers using noise,” *Phys. Rev. A* **108**, 062424 (2023).
- [95] J. C. Owrutsky, D. Raftery, and R. M. Hochstrasser, “Vibrational relaxation dynamics in solutions,” *Annu. Rev. Phys. Chem.* **45**, 519 (1994).
- [96] S. A. Egorov and B. J. Berne, “Vibrational energy relaxation in the condensed phases: Quantum vs classical bath for multiphonon processes,” *J. Chem. Phys.* **107**, 6050 (1997).
- [97] T. Furtenbacher, R. Tóbiás, J. Tennyson, O. L. Polyansky, and A. G. Császár, “W2020: A database of validated rovibrational experimental transitions and empirical energy levels of  $\text{H}_2^{16}\text{O}$ ,” *J. Phys. Chem. Ref. Data* **49**, 033101 (2020).